Research Article

Topological transformation of magnetic hopfion in confined geometries

Yang Gao[1,#] , **Shuang Li[2,#]** , **Yuelei Zhao[2]**, **Zhaozhao Zhu[3]**, **Linyu Cao[1]**, **Jiawang Xu[1]** , **Yan Zhou[2]**, **Shouguo Wang[1]**

[1]Anhui Key Laboratory of Magnetic Functional Materials and Devices, School of Materials Science and Engineering, Anhui University, Hefei 230601, Anhui, China.
[2]School of Science and Engineering, The Chinese University of Hong Kong, Shenzhen 518172, Guangdong, China.
[3]Songshan Lake Materials Laboratory, Dongguan 523808, Guangdong, China.
[#]Authors contributed equally.

Correspondence to: Prof. Yan Zhou, School of Science and Engineering, The Chinese University of Hong Kong, 2001 Longxiang Boulevard, Longgang District, Shenzhen 518172, Guangdong, China. E-mail: zhouyan@cuhk.edu.cn; Prof. Shouguo Wang, School of Materials Science and Engineering, Anhui University, 111 Jiulong Road, Economic and Technological Development District, Hefei 230601, Anhui, China. E-mail: sgwang@ahu.edu.cn

Abstract

Three-dimensional (3D) topological magnetic structures have attracted enormous interest due to their exceptional spatial structures and intriguing physics. Hopfions, characterized by the Hopf index, are 3D spin textures that emerged as closed twisted skyrmion strings. A comprehensive understanding of magnetic structural transitions within nanostructures is crucial for their applications in spintronics devices. Despite the demonstration of stabilization and current-driven dynamics of hopfion, their behavior in geometric confinement has remained unexplored. Here, we investigate the transformation between hopfions and torons in various nanostructures using micromagnetic simulations. By tailoring the axial ratio of elliptical nanodisks, the elliptical hopfion is found to be transformed into a toron structure. Moreover, the current-driven topological transformation between hopfion and toron has also been realized in finite-sized nanostripes and stepped nanostructures. This deformation and transformation arise from the repulsive potential of the boundaries or edges. To connect real-space observations and 3D topological spin configurations, we simulate the Lorentz transmission electron microscope images of the aforementioned magnetic structures. This study, uncovering the dynamics and transformation of hopfions, will invigorate 3D magnetic structures-based memory and logic devices.

Keywords: Hopfion, topological transformation, confined system, micromagnetic simulation

INTRODUCTION

Topological solitons are particle-like objects initially described in effective nonlinear field theories and later introduced to condensed matter systems[1,2]. The continuous winding number of the two-dimensional (2D) solitonic vector field is characterized by a topological charge that classifies various configurations, including skyrmions[3-5], merons[6-8], and skyrmioniums[9,10]. These field configurations have been extensively studied in magnetic materials and promise applications in spintronics. Recent attention has been paid to three-dimensional (3D) topological spin solitons[11-13], among which skyrmion strings[12,14], magnetic bobbers[13,15], skyrmion bundles[16], and emergent magnetic monopoles[17] exhibit intriguing physical properties and nontrivial dynamic responses. Hopfions are 3D topological solitons that emerge when skyrmion strings twist into a torus with distinct knots[18]. Each cross-section of the skyrmion string exhibits the skyrmion structure. By twisting one end of the string through a complete revolution, bending the string, and connecting the two ends to form a circular closed loop, the hopfion structure is formed[19,20]. There are diverse hopfion structures corresponding to different rings, knots, and links that can be classified by the linking number of field lines known as the Hopf index[21,22]. Hopfions have been found in various physical systems, such as fluids[23,24], liquid crystals[25], and optical mediums[26]. In liquid crystals, the transformation between hopfions with different geometric structures has been demonstrated by applying electric fields[27]. Moreover, the inter-transformation of hopfions and torons can be achieved using laser tweezers[28].

Recently, several works revealed hopfions stabilized in noncentrosymmetric magnetic solids with Dzyaloshinskii-Moriya interactions (DMI)[21,29,30] or frustrated magnets with high-order exchange interactions[31]. The experimental study has verified the stabilization of hopfions in Ir/Co/Pt multilayers using X-ray imaging methods[32]. More recently, a deformed skyrmionium with a noninteger Hopf index, also called fractional hopfion, has been observed in a chiral magnetic FeGe through Lorentz transmission electron microscopy (LTEM) techniques[33]. Similar to the clarifications of skyrmions, hopfions are identified with two types, that is, the Bloch-type and Néel-type hopfions. The formation of Bloch-type hopfions is facilitated by bulk DMI, which arises from the broken crystal inversion symmetry[30]. On the other hand, Néel-type hopfions can be formed in the presence of interfacial DMI with broken interface symmetry[32]. Notably, interfacial perpendicular magnetic anisotropy (PMA) is essential in stabilizing both types of hopfions[22]. Besides, the 3D twisted and knotted configurations of hopfions exhibit intriguing properties in their current-driven dynamics[22,31] and resonant modes[34]. Hopfions have a non-zero Hopf charge and exhibit rotational symmetry, while skyrmioniums have zero skyrmion number and lack rotational symmetry[35]. Hopfions are generally more stable due to their higher symmetry and exhibit unique 3D motion free from the boundary constraints, such as translational motion, rotation, and dilation[31]. When subjected to magnetic fields, hopfions transform into torons accompanied by a change in excitation modes[34]. They possess a vanishing gyrovector in a racetrack, making them superior to skyrmions as information carriers because they do not exhibit undesirable skyrmion Hall effects[22]. However, the impact of geometric confinement and boundaries on the behavior of hopfions is often overlooked despite their crucial role in stabilizing hopfions and designing hopfion-based electronic devices.

In this article, we present a numerical investigation of the Bloch-type hopfion in a chiral magnet sandwiched between two layers with high PMA. We explore the statics of hopfions in confined nanodisks with varied shapes and the current-driven dynamics in finite-size rectangular nanostripes with designed nanostructures. Remarkably, the hopfions are found to transform into toron structures due to the repulsive potential from the edge. Furthermore, the LTEM images of versatile configurations are simulated to guide their experimental research. Our work paves the road to hopfion-based memory and logic spintronic devices.

MATERIALS AND METHODS

Micromagnetic simulations

Micromagnetic simulations were performed using the MUMAX3 software package[36], which is widely adopted for simulating various 3D topological magnetic structures. It is a GPU-accelerated operation and can significantly enhance the computational speed, particularly beneficial for handling larger volumes of data. We sandwiched the chiral magnet with a thickness of 78 nm by two 6 nm-thick layers with strong PMA (K_s = 1 MJ/m^2). The initial state was computed from an ansatz[22]. The materials parameters of the chiral magnet layer were taken from FeGe[15,37], M_s = 384 kA/m, A = 4 pJ/m, and D = 0.718 mJ/m^2. The bulk PMA K_b is from 0 to 60 kJ/m^3, and the perpendicular magnetic field H_z is from 0 to 0.44 T. The meshed cell size is 3 nm × 3nm × 2 nm. For the current-driven dynamics, the spin dynamics of hopfion were simulated based on the LLG equation containing the spin-transfer torque (STT) term:

$$\frac{d\mathbf{m}}{dt} = -\gamma \mathbf{m} \times \mathbf{H}_{\text{eff}} + \alpha \mathbf{m} \times \frac{d\mathbf{m}}{dt} + \frac{1}{1+\alpha^2}\{(1+\beta\alpha)\mathbf{m} \times [\mathbf{m} \times (\mathbf{u} \cdot \nabla)\mathbf{m}]$$
$$+ (\beta - \alpha)\mathbf{m} \times (\mathbf{u} \cdot \nabla)\mathbf{m}\}, \tag{1}$$

where γ is the gyromagnetic ratio, $\mathbf{H}_{\text{eff}}$ is the effective field. The second term denotes the Gilbert damping contribution where α is fixed at 0.05. The last two terms describe the coupling between spin and spin-polarized current according to the Zhang-Li STT model. β is the degree of non-adiabaticity. $\mathbf{u} = \mu_B p\mathbf{J}/[eM_s (1 + \beta^2)]$ is the velocity of the conduction electrons, in which p is the spin polarization of the magnet and $\mathbf{J}$ is the current density. Here, we set β = 0.05 and p = 0.3. The value of β/α can influence the STT-driven domain velocity[38], and the parameter p affects spin transfer efficiency, consequently leading to the change of domain-motion velocity. In our study, we selected the α, β, and p values that align with the previous works to simulate the current-driven dynamic in FeGe[37]. The size of the rectangular nanostripe is 900 × 600 nm^2, and the sample thickness is 100 nm. The boundary effect of the plate was considered without setting any periodic boundary conditions.

LTEM simulations

The LTEM images were calculated by using PyLorentz[39], a software tool designed for mapping magnetic structures. The magnetic phase shifts (φ) based on the 3D spin textures were calculated by using the linear superposition method, which directly relates to the magnetization in Fourier space as

$$\varphi = \frac{i\pi\mu_0}{\phi_0}\frac{|\mathbf{M}(\mathbf{k}) \times \mathbf{k}|_z}{k_\perp^2}, \tag{2}$$

where $\mathbf{k}$ represents the position in Fourier space, $k_\perp$ is the position vector in the projection plane within Fourier space, while the z-axis corresponds to the direction of the incident beam. The summation of the phase shifts of each voxel yields the total phase shift, which can be related to the real-space position. To simulate the LTEM images, the magnetization file obtained from MUMAX3 is imported into PyLorentz. The SimTEM code within PyLorentz calculates the electron phase shift based on the input magnetization data, allowing for the simulation of LTEM images with dark and bright contrasts. The magnetic induction can also be reconstructed by using two through focal series via PyLorentz.

RESULTS AND DISCUSSION

3D structures of hopfion and toron

Magnetic hopfions can be formed in a system consisting of a chiral magnet or asymmetric multilayers with one moderate PMA layer sandwiched by two magnetic layers with strong PMA. The free energy terms of this system are given by

$$E = \int \left[A(\nabla \mathbf{m})^2 + \omega_D + K_b \left(1 - m_z^2\right) + \mu_0 H_z M_s \left(1 - m_z\right) + \varepsilon_d \right] dV$$
$$+ \int K_s \left(1 - m_z^2\right) dS, \tag{3}$$

where A is the Heisenberg exchange constant, ω_D is the DMI energy density depending on the symmetry of the system. We consider a chiral magnet with bulk DMI, where $\omega_D = D\mathbf{m} \cdot [\nabla \times \mathbf{m}]$. K_b and K_s are bulk and the interfacial PMA constants, respectively. H_z is the magnetic field applied along the z-axis, M_s is the saturated magnetization and ε_d is the demagnetization energy density. First, we conduct simulations in a square geometry comprising a chiral magnet layer sandwiched by two layers with strong PMA. Consequently, a Bloch-type hopfion is permitted in the absence of an external magnetic field. Figure 1A shows the hopfion preimages of spins with zero perpendicular component (s_z), which represents the iso-surface configurations with zero s_z. The inset of Figure 1A shows the multiple cross-sectional spin texture images in the xy plane at different heights for the hopfion. The magnetization at the top and bottom surfaces is oriented upwards, which is due to the strong PMA in the outer layers. In the vicinity of the upper or lower layers, the hopfion exhibits a toroidal vortex structure with the central spins oriented upwards. The cross-sectional spin texture at the intermediate layers exhibits a Bloch-type skyrmionium[40]. Unlike a skyrmion with a topological charge of one, a skyrmionium is a skyrmion surrounded by an annular domain wall with an opposite topological charge, resulting in a total topological charge of zero. When an external magnetic field H_z is applied, the core spins of the hopfion gradually contract, resulting in the transformation from hopfion into a toron state. Meanwhile, the midplane magnetization profile changes from the skyrmionium to a skyrmion. Figure 1B shows the preimages of a toron with zero s_z at $H_z = 0.2$ T. As shown in the inset of Figure 1B, the toron consists of skyrmion layers aligning across much of the xy plane with a monopole-antimonopole pair located at its upper and lower ends[41]. In addition, the xz midplane cross-sectional spin texture of the hopfion [Figure 1C] is a skyrmion-antiskyrmion pair.

The topological invariant of hopfions in real space, known as the Hopf index[22], can be expressed as

$$Q_H = -\int \mathbf{B} \cdot \mathbf{A} d^3 r, \tag{4}$$

where $B_i = \varepsilon_{ijk} \mathbf{n} \cdot \left(\nabla_j \mathbf{n} \times \nabla_k \mathbf{n}\right)/8\pi$ is the emergent magnetic field calculated from the unit vector field $\mathbf{n}$, and $\mathbf{A}$ is the emergent vector potential that satisfies the equation $\nabla \times \mathbf{A} = \mathbf{B}$. The Hopf index can also be calculated using the linking number of knots, determined by their toroidal (T) and poloidal (P) cycles. The Hopf index is therefore given by $Q_H = \text{TP}$[21]. Accordingly, the Q_H in Figure 1A is calculated at approximately 1. However, the Hopf invariant is ill-defined for the toron due to the presence of two monopoles near two surfaces that induce the unsmooth distribution of $\mathbf{B}$. In the presence of strong perpendicular boundary conditions in confined surfaces, the skyrmion tube ends with two monopoles, each carrying opposite charges[42]. Moreover, within the planes between the confined surfaces, the cross-sectional spin texture of the toron exhibits an elementary skyrmion. Since the 3D hopfion and toron are constructed from multiple layers exhibiting an independent 2D spin texture, analyzing their layer-dependent 2D topological charge enables differentiation between these two structures. The 2D topological charge is defined as
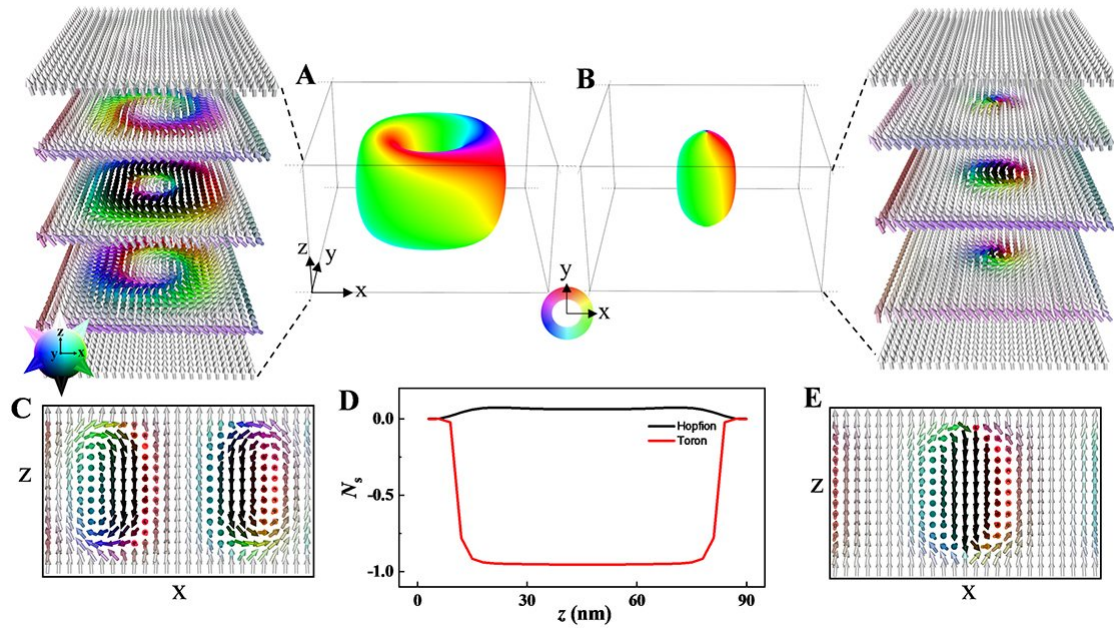
Figure 1. 3D topological spin textures of hopfions and torons. The set of preimages with $s_z = 0$ for hopfions at 0 T (A) and toron at 0.2 T (B) in a square domain with side length L = 150 nm and thickness t = 90 nm. The preimage refers to a mapping of the 3D space that contains spins with the same orientations. The left and right insets show the series of cross-sectional spin textures for the hopfion and the toron in the xy plane, respectively. The color sphere denotes the spin orientation in three dimensions. The color wheel denotes the spin orientation in the xy plane. (C) The xz midplane cross-section of the hopfion. (D) The dependence of the 2D topological charge (N_s) on the perpendicular position z for the hopfion and the toron. (E) The xz midplane cross-section of the toron.

$N_s = \frac{1}{4\pi} \int \mathbf{n} \cdot \left(\partial_x \mathbf{n} \times \partial_y \mathbf{n} \right) d^2 r$. Figure 1D shows the layer dependence of the N_s for the hopfion and the toron, both of which have a zero topological charge on the top and bottom surfaces due to the surface pinning from strong PMA layers. The xz midplane cross-sectional spin texture of the toron is shown in Figure 1E. In the middle plane with weak PMA, the N_s of the hopfion remains 0, while the toron changes from 0 to 1. This result is consistent with the aforementioned 2D magnetization profiles, where the topological charges of skyrmionium and skyrmion are 0 and 1, respectively.

Hopfions in nanodisks with various outer boundary shapes

To gain more insight into how boundary geometry influences the topological transformation of the 3D magnetic structure, we analyze the spin configurations at zero fields in confined systems with various outer boundary shapes. The formation of hopfion stems from the competition terms in Eq. 3, where demagnetization energy is largely impacted by the confined geometric shape. When a hopfion is confined within a square geometry, it adopts a square shape [Figure 1A], while it turns into a circular shape in a circular nanodisk [Figure 2A]. Although the morphology of hopfions is altered by the shape of the geometric constraint, their topology remains unchanged with a linking number of knots that equals 1, which is consistent with a previous study[29]. In order to facilitate experimental observation of hopfions, we simulate LTEM images that highlight their in-plane spin component. Their simulated phase-shift and under-focused LTEM images viewed along the z-axis in circular nanodisk are shown in Figure 2B and C, respectively. The LTEM images of a hopfion at different focus setting is shown in Supplementary Figure 1. Figure 2D shows the reconstruction of the magnetic component distribution of hopfions by solving the transport-of-intensity equation (TIE) via focal series, in line with the in-plane spin distribution depicted in Figure 2A. An under-focus image displays a ring-like pattern with a bright circular hola surrounding a dark spot, which is distinct from the LTEM contrasts of skyrmion tubes or bobbers, which only show a bright
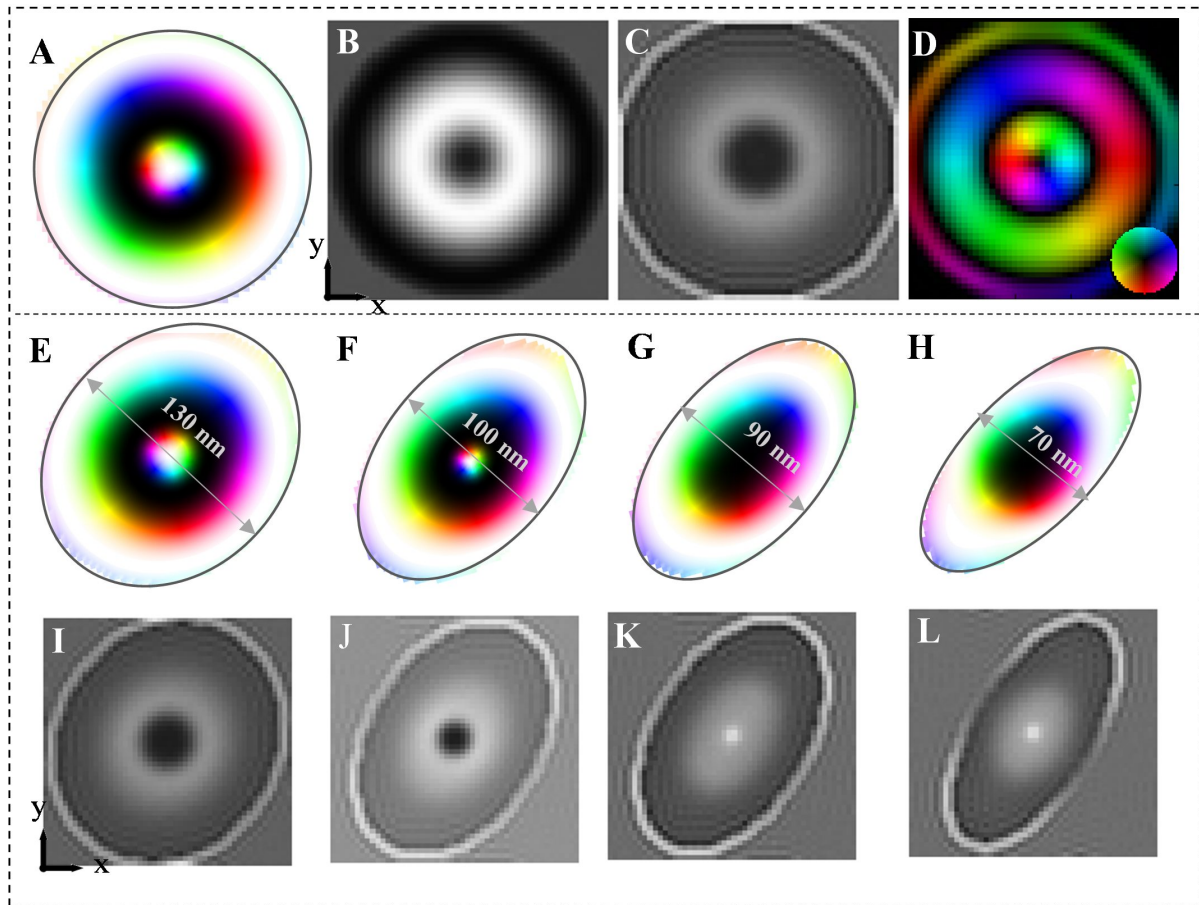
Figure 2. Hopfion under geometric constriction. (A) Mid-plane cross-sections of hopfions in circular nanodisk with d = 150 nm. (B) Simulated phase-shift image and (C) under-focused LTEM image of hopfion shown in (A) for viewing directions along the z-axis. (D) In-plane magnetic component distribution reconstructed by solving the transport-of-intensity equation. (E-H) Magnetization structures stabilized in elliptical nanodisks with different short axis lengths at the mid-plane. (I-L) Results of simulated under-focused LTEM images in elliptical nanodisks corresponding to hopfions in (E-H).

spot[15]. However, the ring pattern observed in an under-focused hopfion image may resemble that of a skyrmionium tube with a ring pattern, and the comparison of phase intensity between the two textures is addressed in Supplementary Figure 2[43].

Recently, several studies have delved into the existence and stability of elliptical skyrmions, which showcase exceptional dynamics and resonance modes through the implementation of anisotropic DMI and anisotropic magnetic anisotropy[44-46]. Here, we find that the elliptical hopfion can be formed via geometric constraints. Figure 2E-H presents an overview of the relaxed magnetic configurations in elliptical nanodisks with varying axial ratios, where the long axis (LA) length is fixed at 150 nm and the short axis (SA) length varies at 130 nm [Figure 2E], 100 nm [Figure 2F], 90 nm [Figure 2G], and 70 nm [Figure 2H]. When the SA length is greater than 100 nm, the elliptical hopfion remains stable. However, as it decreases below 100 nm, the hopfion undergoes a gradual transformation into a toron state, which is attributed to the boundary effect. It should be noted that the demagnetizing fields play a crucial role in determining the stability of 3D textures with diverse geometric shapes, which is further demonstrated in Supplementary Figure 3. Figure 2I-L presents the simulated under-focused LTEM images in elliptical nanodisks corresponding to the magnetic configuration in Figure 2E-H. LTEM images with distinct contrast can reproduce hopfion transformation.

The dark central spots in Figure 2I and J represent the core spin arrangement of hopfions, while the central shiny point in Figure 2K and L indicates the position of the Bloch points of the toron with a deeper magnetic length. Thus, careful observation of LTEM contrast can reveal detailed information about these topological textures. For the real-space observation of these topological textures, a promising system involves combining chiral magnets with magnetic multilayers. Specifically, multilayer systems, such as Ta/CoFeB/MgO[47], Pt/Co/Ta[48], and Pt/Co/Ir[32], allow for tunable PMA by adjusting the ferromagnetic layer thickness and stack configuration. The fabrication of heterostructures by incorporating chiral magnets such as FeGe[49], $Co_9Zn_9Mn_2$[50], and Cu_3OSeO_3[13] sandwiched between multilayers possessing high PMA holds great promise for this purpose.

Current-driven motion of hopfion in a nonostripe

In comparison with the nanodisk, understanding hopfion behavior and stability within a nanostripe contributes to their application in racetrack memory. Figure 3 illustrates typical metastable states in a finite-size nanostripe with different values of K_b and H_z. A wide range of K_b (0-60 KJ/m³) and H_z (0.20-0.40 T) allows for the stabilization of hopfion, which indicates that the formation of the topological structure is not parameter-sensitive and appears to be widespread. Low K_b values result in an in-plane magnetic background, and small H_z values lead to the formation of stripe domains. This occurs because the enlarged hopfions reach the boundary and knots break. With an increase in H_z, the radius of a hopfion gradually shrinks, and it changes into a toron structure and eventually transitions to a ferromagnetic uniform state.

According to the above results, the shape confinement effect in small-scale nanodisks enables the stable existence of hopfion at zero fields. In nanostripes or thin plates, hopfions exist as a metastable state and require an assistant magnetic field. Given the potential application of hopfions in racetrack memory, understanding their stability and current-induced dynamics within a nanostripe is crucial. Figure 4A shows the relaxed state at K_b = 40 kJ/m³ and H_z = 0.34 T, with the hopfion initially located at the left side of the nanostripe. The hopfion eventually stabilizes near the center of the nanostripe due to the repulsive force from the surrounding borders[51]. It was found that as the length of the nanostripe increases, the hopfion can also stabilize on the left side of the stripe. Detailed information regarding the relationship between the hopfion and its distance from the boundary as the length varied is available in Supplementary Figure 4. When applying a current with J = -8 × 10¹¹ A·m⁻² along the x direction, the hopfion first moves against the spin-polarized current direction for a short distance via STT. Subsequently, the hopfion slightly bounces back and eventually comes to a halt at a position approximately 300 nm away from the right boundary [Supplementary Movie 1]. It fails to reach the boundary owing to the large repulsive force from the edge, a phenomenon similar to that observed in skyrmion-host systems[38]. For a larger current density J = -10 × 10¹¹ A·m⁻², hopfions can overcome the potential barrier and reach the boundary, as demonstrated in Figure 4A-D. The threshold current density J_c to overcome the boundary barrier is -8.9 × 10¹¹ A·m⁻² in the nanostripe at 0.34 T. Hopfions move straight initially [Figure 4B] and gradually deform [Figure 4C] as they approach the right boundary. Thereafter, the deformed hopfion transforms into the toron structure [Figure 4D] with the collapse of core spins, ultimately leading to its annihilation at the sample edge. The corresponding motion and transition processes are shown in Supplementary Movie 2. Magnetic contrasts of LTEM images for the current-driven motion of hopfion are presented in Figure 4E-H. The conversion of the magnetic contrasts from a ring-like pattern [Figure 4E-G] to a bright spot [Figure 4H] identifies the topological transition process. Different from the direct annihilation of skyrmion at the edge under an electric current, we find that hopfion undergoes a topological transition into toron before annihilation due to the combined effect of STT and the repulsive potential from the boundary. The driving force from STT and the repulsive force from the boundary exert a compression effect on the hopfion, thereby causing its distortion into a toron.
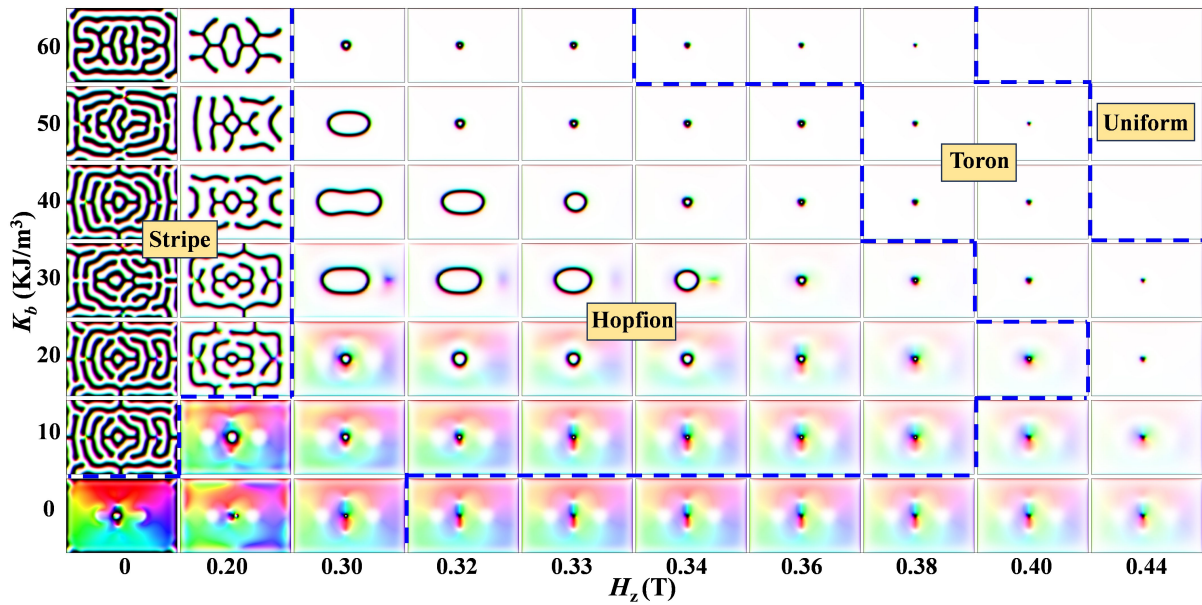
Figure 3. Phase diagram of different topological states with respect to PMA constant K_b and perpendicular magnetic field H_z. The metastable states are obtained by relaxing the magnetic nanostripe with an initial hopfion state at the center. The midplane ($z = 50$ nm) cross-sections of **m** are presented. The size of the nanostripe is $900 \times 600 \times 100$ nm^3.

The motion of hopfion can be qualitatively described within the framework of Thiele's equation

$$\mathbf{G} \times (\mathbf{v} - \mathbf{u}) + \boldsymbol{D} \cdot (\alpha \mathbf{v} - \beta \mathbf{u}) + \mathbf{F} = 0. \tag{5}$$

The first term denotes the Magnus force, $\mathbf{G} = (0, 0, 4\pi N_s)$ is the gyrovector, $\mathbf{v}$ is the velocity of the hopfion, and $\mathbf{u}$ is the STT-related electron driving velocity. The second term represents the dissipation force related to the tensor D defined as $D_{ij} = \int \partial_i \mathbf{m} \cdot \partial_j \mathbf{m} dV$. The third term $\mathbf{F}$ is the force acting on the hopfion, which mainly comes from the interaction from the surrounding boundaries in our case. Due to a vanishing gyrovector, hopfions can move along the current via STT according to Eq. 3. However, for intermediate layers of toron, N_s are non-zero, which means that the Magnus force cannot be neglected and may induce a transversal motion of the toron. Figure 4I displays the trajectory of the local spin texture induced by current during a period of 15 ns; the position is determined by calculating the guiding center R(X, Y) of spin textures, expressed as $R(X,Y) = 1/4\pi N_s \int i\mathbf{n} \cdot (\partial_x \mathbf{n} \times \partial_y \mathbf{n}) dxdy$, $i = x, y$. The hopfion exhibits straight motion along the x direction, whereas the toron shifts to the -y direction, consistent with the analysis presented above. Note that the slight +y direction deviation of the hopfion at about 630 nm is caused by its deformation. Figure 4J shows the longitudinal component of the soliton velocity v_x and 2D topological charge N_s in the midplane as a function of time t. Owning to the repulsive force from the edge, hopfion shows a gradual decrease in v_x before the transformation (1-10 ns). During the period of current-driven transition from a hopfion to toron (10-12 ns), the N_s of the midplane changes from 0 to 1 and v_x increases significantly and maintains a relatively large value until it is annihilated at the edge (12-16 ns). Besides, the toron structure can be formed by only increasing the applied magnetic field from 0.34 to 0.38 T. More details about the current-driven toron in the nanostripe are shown in Supplementary Figure 5 and Supplementary Movie 3. The repulsive potential from the boundary is mainly induced by the chiral edge state, which represents the twist of the spin and nearly-in-plane spins at the edge of the nanostripe. Such edge state has been quantitatively verified in chiral magnets[52]. To further illustrate this, Figure 4K presents the distribution of the demagnetization
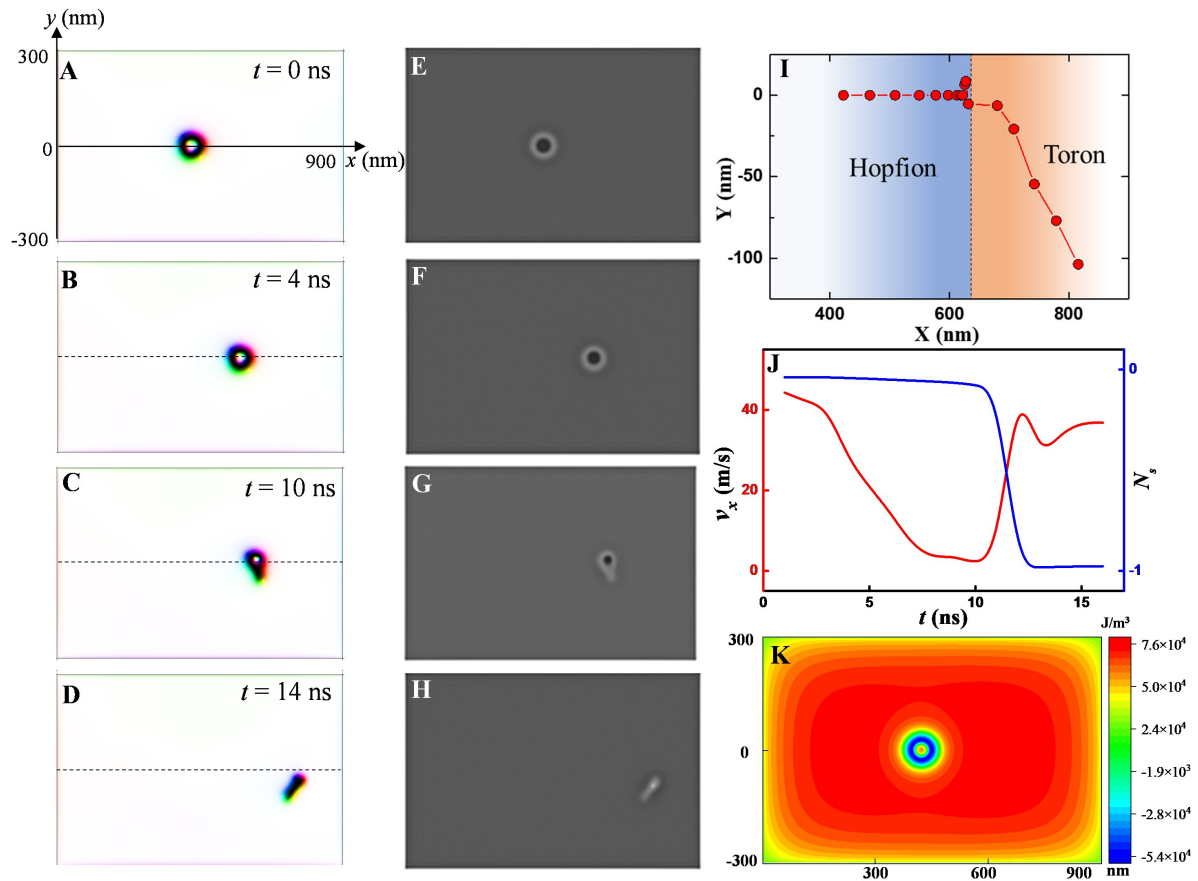
Figure 4. Current-driven hopfion motion by STT in a nanostripe. (A-D) Current-driven motions of a hopfion at **J** = -10 × 10^{11} A·m^{-2} under a magnetic field of 0.34 T. The size of the simulated region is 900 × 600 × 100 nm^3. The midplane (z = 50nm) cross-sections of **m** are shown. (E-H) Simulated under-focused LTEM images corresponding to structures in (A-D). (I) Trajectory of the spin texture driven by STT during a period of 16 ns. (J) The hopfion motion velocity along the x-axis v_x and 2D topological number N_s as a function of time t. The v_x and N_s are calculated based on spin textures in the midplane. (K) The demagnetizing energy density in the z = 50 nm plane at 0 ns.

energy densities for the spin configurations depicted in Figure 4A. The energy in the interior zone is stronger than that at the edge, coinciding with the perpendicular spin alignment at the intermediate region and in-plane tilted spin distribution at the edge.

Current-driven hopfion in artificially designed nanostructures

Finally, we study the current-driven dynamics of hopfions in artificially designed nanostructures, including a nanostripe with a single square notch, "H-like" shaped configurations, and stepped nanostructures. Figure 5A illustrates the motion of the hopfion in the nanostripe with a single-notch structure. The size of the notch is 60 nm × 150 nm and the hopfion trajectory is depicted by the black dashed line. Due to the extra repulsive force introduced by the notch, the hopfion stabilizes at the left side instead of the center of the nanostripe. When applying a current with **J** = -10 × 10^{11} A·m^{-2}, the hopfion initially moves straightly along the +x direction and then shifts away from the notch. As the hopfion traverses the notch, it shifts back due to the diminished influence from the notch. The dynamical response of hopfion when approaching the boundary is similar to what is discussed in the case of the nanostripe. For the "H-like" nanostripe featuring two symmetrical notches of dimensions 150 nm × 150 nm, the hopfion moves almost entirely along the x direction with minimal deviation [Figure 5B]. This result is anticipated, given the canceled repulsive forces
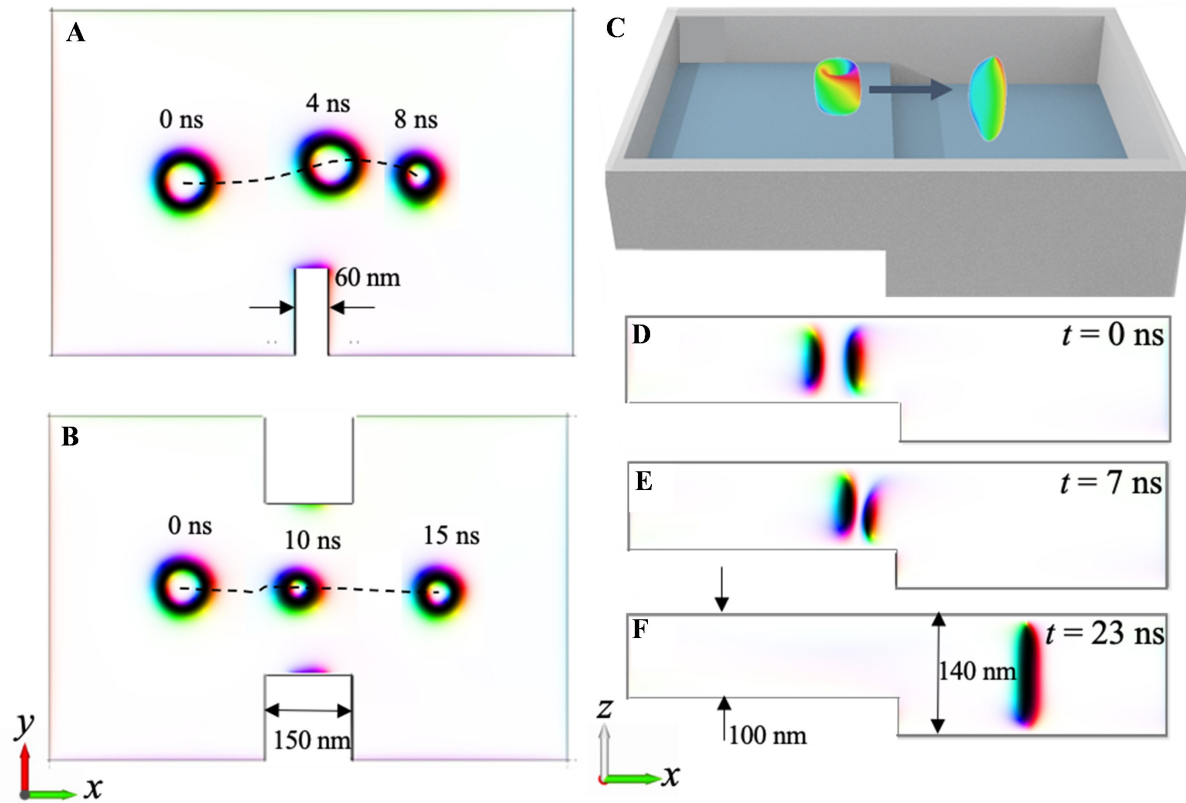
Figure 5. Current-driven dynamics of hopfions in designed nanostructures. Trajectory of hopfions in (A) nanostripe with a single notch. (B) "H-like" shaped nanostructures at J = -10 × 10^{11} A·m^{-2}. (C) Current-driven transition from hopfion to toron in a stepped geometry at J = -10 × 10^{11} A·m^{-2}. The cross-sectional spin textures in the *xz* plane show (D) a hopfion, (E) a distorted hopfion, and (F) a toron structure at different times.

from the top and bottom notches. However, the hopfion experiences compression when traveling between the notches, leading to a reduction in its size. This indicates that introducing specific shapes of nanostructures can significantly alter the current-driven trajectory and size of the hopfions.

Taking inspiration from previous work on the transformation between a skyrmion tube and bobber in a stepped nanostructure[37], we investigate the current-driven dynamics of hopfion in a nanostripe containing a vertical step, where a topological transformation potentially takes place. Figure 5C schematically shows the motion of the hopfion in a stepped geometry, and the cross-sectional spin textures in the *xz* plane are shown in Figure 5D-F, depicting the transformation from hopfion to toron in the stepped nanostructure. As the hopfion approaches the step edge, the potential barrier induces the hopfion to distort [Figure 5E], and finally, a toron forms in the thicker region [Figure 5F]. Unlike the toron state that occurs after a topological transition near the boundary or notch, each topological state in the stepped nanostructure can be easily generated and is capable of traveling long distances.

Studying the interaction between 3D topological spin textures and the sample geometry presents an effective strategy for addressing their stability and tunability[53,54]. Additionally, topological transformations hold immense potential for spintronic applications and could lead to the emergence of novel practical uses based on diverse 3D topological structures. The polarity of vortices[55], topological charge[56], and other topological quantities[57] are found to be altered by various external stimuli, including magnetic field pulses,

in-plane magnetic fields, and thermal energy. In comparison to the topological phase transitions induced by the aforementioned methods, the transitions of 3D topological spin textures caused by geometric shapes and currents discovered in this study make it easier to integrate them into spintronic devices, which can then be used to control the size and motion trajectory of topological spin textures. The reliable transformation from hopfion to toron makes the 3D topological magnetic structures act as reliable information carriers that can be applied to (i) hopfion racetrack memory enabling binary bit states[37]; (ii) magnetic memories for temporal computing[58]; and (iii) artificial synapses and neurons[59]. However, the nucleation of hopfions within nanostripes or nanoflakes remains challenging in experiments. For the formation of hopfion, two potential methods could be considered: Injecting an annular spin polarized current to reverse the local magnetization and facilitate hopfion creation; Applying positive and negative magnetic fields to induce hopfion formation. Moreover, for practical applications in devices, the hopfion-hopfion interaction and their interaction with defects should be further investigated.

CONCLUSIONS

In summary, this work provides a simulated exploration of the Bloch-type hopfion in chiral magnets, including its stability, current-driven behavior, and topological transformation in confined systems of finite size. Various approaches for inducing the topological transformation have been demonstrated, including the application of magnetic fields, confinement of shapes, and the employment of currents in combination with boundary or artificial edge potentials. Computer-simulated LTEM images of spin configurations are also included to assist in guiding experimental research in magnetic solids. Our findings significantly enhance the comprehension of the behavior exhibited by these fascinating 3D topological magnetic structures.

DECLARATIONS

Authors' contributions
Conceived and designed the study: Zhou Y, Wang S
Performed data analysis and wrote the main draft of the paper: Gao Y, Li S, Zhu Z, Cao L
Provided technical support: Zhao Y, Xu J
All authors discussed the results and commented on the manuscript.

Availability of data and materials
Not applicable.

Conflicts of interest
All authors declared that there are no conflicts of interest.

Ethical approval and consent to participate

Not applicable.

Consent for publication

Not applicable.

Copyright

© The Author(s) 2024.

REFERENCES

1. Skyrme THR. A non-linear field theory. *Proc R Soc Lond A* 1961;260:127-38. DOI
2. Battye RA, Sutcliffe PM. Knots as stable soliton solutions in a three-dimensional classical field theory. *Phys Rev Lett* 1998;81:4798. DOI
3. Fert A, Cros V, Sampaio J. Skyrmions on the track. *Nat Nanotechnol* 2013;8:152-6. DOI PubMed
4. Tonomura A, Yu XZ, Yanagisawa K, et al. Real-space observation of skyrmion lattice in helimagnet MnSi thin samples. *Nano Lett* 2012;12:1673-7. DOI
5. Zhou Y. Magnetic skyrmions: intriguing physics and new spintronic device concepts. *Natl Sci Rev* 2019;6:210-2. DOI PubMed PMC
6. Li X, Shen L, Bai Y, et al. Bimeron clusters in chiral antiferromagnets. *NPJ Comput Mater* 2020;6:169. DOI
7. Lin SZ, Saxena A, Batista CD. Skyrmion fractionalization and merons in chiral magnets with easy-plane anisotropy. *Phys Rev B* 2015;91:224407. DOI
8. Gao Y, Yin QW, Wang Q, et al. Spontaneous (Anti)meron chains in the domain walls of van der Waals Ferromagnetic $Fe_{5-x}GeTe_2$. *Adv Mater* 2020;32:e2005228. DOI
9. Kolesnikov AG, Stebliy ME, Samardak AS, Ognev AV. Skyrmionium - high velocity without the skyrmion Hall effect. *Sci Rep* 2018;8:16966. DOI PubMed PMC
10. Göbel B, Schäffer AF, Berakdar J, Mertig I, Parkin SSP. Electrical writing, deleting, reading, and moving of magnetic skyrmioniums in a racetrack device. *Sci Rep* 2019;9:12119. DOI PubMed PMC
11. Wolf D, Schneider S, Rößler UK, et al. Unveiling the three-dimensional magnetic texture of skyrmion tubes. *Nat Nanotechnol* 2022;17:250-5. DOI PubMed PMC
12. Seki S, Suzuki M, Ishibashi M, et al. Direct visualization of the three-dimensional shape of skyrmion strings in a noncentrosymmetric magnet. *Nat Mater* 2022;21:181-7. DOI
13. Ran K, Liu Y, Guang Y, et al. Creation of a chiral bobber lattice in helimagnet-multilayer heterostructures. *Phys Rev Lett* 2021;126:017204. DOI
14. Seki S, Garst M, Waizner J, et al. Propagation dynamics of spin excitations along skyrmion strings. *Nat Commun* 2020;11:256. DOI PubMed PMC
15. Zheng F, Rybakov FN, Borisov AB, et al. Experimental observation of chiral magnetic bobbers in B20-type FeGe. *Nat Nanotechnol* 2018;13:451-5. DOI
16. Tang J, Wu Y, Wang W, et al. Magnetic skyrmion bundles and their current-driven dynamics. *Nat Nanotechnol* 2021;16:1086-91. DOI
17. Guang Y, Ran K, Zhang J, et al. Superposition of emergent monopole and antimonopole in CoTb thin films. *Phys Rev Lett* 2021;127:217201. DOI
18. Sutcliffe P. Skyrmion knots in frustrated magnets. *Phys Rev Lett* 2017;118:247203. DOI PubMed
19. Wu JS, Smalyukh II. Hopfions, heliknotons, skyrmions, torons and both abelian and nonabelian vortices in chiral liquid crystals. *Liq Cryst Rev* 2022;10:34-68. DOI
20. Raftrey D, Fischer P. Field-driven dynamics of magnetic hopfions. *Phys Rev Lett* 2021;127:257201. DOI PubMed
21. Tai JB, Smalyukh II. Static hopf solitons and knotted emergent fields in solid-state noncentrosymmetric magnetic nanostructures. *Phys Rev Lett* 2018;121:187201. DOI PubMed
22. Wang XS, Qaiumzadeh A, Brataas A. Current-driven dynamics of magnetic hopfions. *Phys Rev Lett* 2019;123:147203. DOI PubMed
23. Kleckner D, Irvine WTM. Creation and dynamics of knotted vortices. *Nat Phys* 2013;9:253-8. DOI
24. Ackerman PJ, Smalyukh II. Static three-dimensional topological solitons in fluid chiral ferromagnets and colloids. *Nat Mater* 2017;16:426-32. DOI PubMed
25. Tai JB, Ackerman PJ, Smalyukh II. Topological transformations of Hopf solitons in chiral ferromagnets and liquid crystals. *Proc Natl Acad Sci USA* 2018;115:921-6. DOI PubMed PMC
26. Sugic D, Droop R, Otte E, et al. Particle-like topologies in light. *Nat Commun* 2021;12:6785. DOI PubMed PMC
27. Tai JB, Wu JS, Smalyukh II. Geometric transformation and three-dimensional hopping of Hopf solitons. *Nat Commun* 2022;13:2986. DOI PubMed PMC
28. Chen BG, Ackerman PJ, Alexander GP, Kamien RD, Smalyukh II. Generating the hopf fibration experimentally in nematic liquid crystals. *Phys Rev Lett* 2013;110:237801. DOI PubMed

29. Liu Y, Lake RK, Zang J. Binding a hopfion in a chiral magnet nanodisk. *Phys Rev B* 2018;98:174437. DOI

30. Sutcliffe P. Hopfions in chiral magnets. *J Phys A Math Theor* 2018;51:375401. DOI

31. Liu Y, Hou W, Han X, Zang J. Three-dimensional dynamics of a magnetic hopfion driven by spin transfer torque. *Phys Rev Lett* 2020;124:127204. DOI

32. Kent N, Reynolds N, Raftrey D, et al. Creation and observation of Hopfions in magnetic multilayer systems. *Nat Commun* 2021;12:1562. DOI PubMed PMC

33. Yu X, Liu Y, Iakoubovskii KV, et al. Realization and current-driven dynamics of fractional hopfions and their ensembles in a helimagnet FeGe. *Adv Mater* 2023;35:e2210646. DOI

34. Li S, Xia J, Shen L, Zhang X, Ezawa M, Zhou Y. Mutual conversion between a magnetic Néel hopfion and a Néel toron. *Phys Rev B* 2022;105:174407. DOI

35. Zhang X, Xia J, Zhou Y, et al. Control and manipulation of a magnetic skyrmionium in nanostructures. *Phys Rev B* 2016;94:094420. DOI

36. Vansteenkiste A, Leliaert J, Dvornik M, Helsen M, Garcia-sanchez F, Van Waeyenberge B. The design and verification of MuMax3. *AIP Adv* 2014;4:107133. DOI

37. Zhu J, Wu Y, Hu Q, et al. Current-driven transformations of a skyrmion tube and a bobber in stepped nanostructures of chiral magnets. *Sci China Phys Mech Astron* 2021;64:227511. DOI

38. Iwasaki J, Mochizuki M, Nagaosa N. Current-induced skyrmion dynamics in constricted geometries. *Nat Nanotechnol* 2013;8:742-7. DOI PubMed

39. Mccray AR, Cote T, Li Y, Petford-long AK, Phatak C. Understanding complex magnetic spin textures with simulation-assisted lorentz transmission electron microscopy. *Phys Rev Appl* 2021;15:044025. DOI

40. Zheng F, Li H, Wang S, et al. Direct imaging of a zero-field target skyrmion and its polarity switch in a chiral magnetic nanodisk. *Phys Rev Lett* 2017;119:197205. DOI

41. Hu Q, Lyu B, Tang J, Kong L, Du H, Wang W. Unidirectional current-driven toron motion in a cylindrical nanowire. *Appl Phys Lett* 2021;118:022404. DOI

42. Zhao H, Malomed BA, Smalyukh II. Topological solitonic macromolecules. *Nat Commun* 2023;14:4581. DOI PubMed PMC

43. Niitsu K, Liu Y, Booth AC. Geometrically stabilized skyrmionic vortex in FeGe tetrahedral nanoparticles. *Nat Mater* 2022;21:305-10. DOI

44. Liu Y, Lake RK, Zang J. Shape dependent resonant modes of skyrmions in magnetic nanodisks. *J Magn Magn Mater* 2018;455:9-13. DOI

45. Xia J, Zhang X, Ezawa M, Shao Q, Liu X, Zhou Y. Dynamics of an elliptical ferromagnetic skyrmion driven by the spin-orbit torque. *Appl Phys Lett* 2020;116:022407. DOI

46. Cui B, Yu D, Shao Z, et al. Néel-type elliptical skyrmions in a laterally asymmetric magnetic multilayer. *Adv Mater* 2021;33:e2006924. DOI

47. Jiang W, Upadhyaya P, Zhang W, et al. Magnetism. Blowing magnetic skyrmion bubbles. *Science* 2015;349:283-6. DOI

48. He M, Li G, Zhu Z, et al. Evolution of topological skyrmions across the spin reorientation transition in Pt/Co/Ta multilayers. *Phys Rev B* 2018;97:174419. DOI

49. Yu XZ, Kanazawa N, Onose Y, et al. Near room-temperature formation of a skyrmion crystal in thin-films of the helimagnet FeGe. *Nat Mater* 2011;10:106-9. DOI

50. Peng L, Karube K, Taguchi Y, Nagaosa N, Tokura Y, Yu X. Dynamic transition of current-driven single-skyrmion motion in a room-temperature chiral-lattice magnet. *Nat Commun* 2021;12:6797. DOI PubMed PMC

51. Wu Y, Jiang J, Tang J. Current-driven dynamics of skyrmion bubbles in achiral uniaxial magnets. *Chinese Phys B* 2022;31:077504. DOI

52. Song D, Li ZA, Caron J, et al. Quantification of magnetic surface and edge states in an FeGe nanostripe by off-axis electron holography. *Phys Rev Lett* 2018;120:167204. DOI

53. Peng L, Iakoubovskii KV, Karube K, Taguchi Y, Tokura Y, Yu X. Formation and control of zero-field antiskyrmions in confining geometries. *Adv Sci* 2022;9:e2202950. DOI PubMed PMC

54. Jena J, Göbel B, Hirosawa T, et al. Observation of fractional spin textures in a Heusler material. *Nat Commun* 2022;13:2348. DOI PubMed PMC

55. Hertel R, Gliga S, Fähnle M, Schneider CM. Ultrafast nanomagnetic toggle switching of vortex cores. *Phys Rev Lett* 2007;98:117201. DOI PubMed

56. Peng L, Takagi R, Koshibae W, et al. Controlled transformation of skyrmions and antiskyrmions in a non-centrosymmetric magnet. *Nat Nanotechnol* 2020;15:181-6. DOI

57. Yu XZ, Shibata K, Koshibae W, et al. Thermally activated helicity reversals of skyrmions. *Phys Rev B* 2016;93:134417. DOI

58. Vakili H, Sakib MN, Ganguly S, et al. Temporal memory with magnetic racetracks. *IEEE J Explor Solid State* 2020;6:107-15. DOI

59. Song KM, Jeong J, Pan B, et al. Skyrmion-based artificial synapses for neuromorphic computing. *Nat Electron* 2020;3:148-55. DOI